Stem Cell Reports
Article

ISSCR

OPEN ACCESS

Surgical Transplantation of Human RPE Stem Cell-Derived RPE Monolayers into Non-Human Primates with Immunosuppression

Zengping Liu,[1,2,3,10] Bhav Harshad Parikh,[1,2,10] Queenie Shu Woon Tan,[1] Daniel Soo Lin Wong,[2] Kok Haur Ong,[1] Weimiao Yu,[1] Ivan Seah,[4] Graham E. Holder,[2,4,7] Walter Hunziker,[1,8] Gavin S.W. Tan,[3,9] Veluchamy Amutha Barathi,[2,3,9] Gopal Lingam,[2,3,4] Boris V. Stanzel,[2,5,*] Timothy A. Blenkinsop,[6,*] and Xinyi Su[1,2,3,4,*]

[1]Institute of Molecular and Cell Biology (IMCB), Agency for Science, Technology and Research (A*STAR), Singapore, Singapore
[2]Department of Ophthalmology, Yong Loo Lin School of Medicine, National University of Singapore, Singapore, Singapore
[3]Singapore Eye Research Institute (SERI), Singapore, Singapore
[4]Department of Ophthalmology, National University Hospital, Singapore, Singapore
[5]Macula Center Saar, Eye Clinic Sulzbach, Knappschaft Hospital Saar, Sulzbach, Saar, Germany
[6]Department of Cellular, Developmental and Regenerative Biology, Icahn School of Medicine at Mount Sinai, New York, NY, USA
[7]UCL Institute of Ophthalmology, London, UK
[8]Department of Physiology, Yong Loo Lin School of Medicine, National University of Singapore, Singapore, Singapore
[9]Academic Clinical Program in Ophthalmology, Duke-NUS Medical School, Singapore, Singapore
[10]These authors contributed equally
*Correspondence: boris.stanzel@kksaar.de (B.V.S.), timothy.blenkinsop@mssm.edu (T.A.B.), xysu@imcb.a-star.edu.sg (X.S.)
https://doi.org/10.1016/j.stemcr.2020.12.007

SUMMARY

Recent trials of retinal pigment epithelium (RPE) transplantation for the treatment of disorders such as age-related macular degeneration have been promising. However, limitations of existing strategies include the uncertain survival of RPE cells delivered by cell suspension and the inherent risk of uncontrolled cell proliferation in the vitreous cavity. Human RPE stem cell-derived RPE (hRPESC-RPE) transplantation can rescue vision in a rat model of retinal dystrophy and survive in the rabbit retina for at least 1 month. The present study placed hRPESC-RPE monolayers under the macula of a non-human primate model for 3 months. The transplant was able to recover *in vivo* and maintained healthy photoreceptors. Importantly, there was no evidence that subretinally transplanted monolayers underwent an epithelial-mesenchymal transition. Neither gliosis in adjacent retina nor epiretinal membranes were observed. These findings suggest that hRPESC-RPE monolayers are safe and may be a useful source for RPE cell replacement therapy.

INTRODUCTION

The retinal pigment epithelium (RPE) is a single-layer epithelium present under the neurosensory retina and is essential for vision. Estimates suggest there are more than 200 million individuals with vision loss due to RPE-related diseases (Wong et al., 2014), reflecting the multiple roles that the RPE has in the maintenance of normal visual transduction. Those roles include provision of the outer blood-retina barrier, management of fluid transport, regulation of cytokine release, processing of reactive oxygen species, recycling of phototransduction components, and regulation of the subretinal space ionic balance (Bharti et al., 2011; Bonilha et al., 2006; Sparrow et al., 2010; Strauss, 2005).

The clinical trials of RPE transplantation as a "cell replacement therapy" for vision-threatening complications of age-related macular degeneration (AMD) showed some preliminary signs of success (da Cruz et al., 2018; Kashani et al., 2018; Mandai et al., 2017; Singh et al., 2020). Cell replacement involves the provision of healthy RPE cells to replace those that are dysfunctional, with the goal of restoring physiological function to the retina. In the case of advanced geographic atrophy (GA) in AMD, wherein both photoreceptors and RPE are lost, RPE replacement aims to prevent further atrophy and, thereby, additional visual loss. Moreover, if dormant photoreceptor nuclei are present within the atrophic area (Bird et al., 2014; Kashani et al., 2018), limited recovery of visual function might also be possible, dependent upon on the extent of damage prior to transplant.

Previous successes with autologous RPE replacements, such as peripheral RPE/choroid patch and macular translocation, laid the foundation for stem cell-based RPE therapy (Stanga et al., 2002; van Zeeburg et al., 2012). Notwithstanding guarded visual outcomes, those early approaches had limited uptake due to the complexity of the surgical procedures, resulting in the search for alternative stem cell-based RPE sources for clinical applications. Recent clinical trials on eye disease have demonstrated promising results using human embryonic stem cell (hESC)-RPE and human induced pluripotent stem cell (iPSC)-RPE (da Cruz et al., 2018; Mandai et al., 2017; Schwartz et al., 2012; Schwartz et al., 2015). Human RPE stem cell-derived RPE (hRPESC-RPE) is an additional, potentially unlimited cell source of human leukocyte antigen (HLA) matching and an unlimited donor source with some qualities favorable to translation, including stability, ubiquity, and cost. A

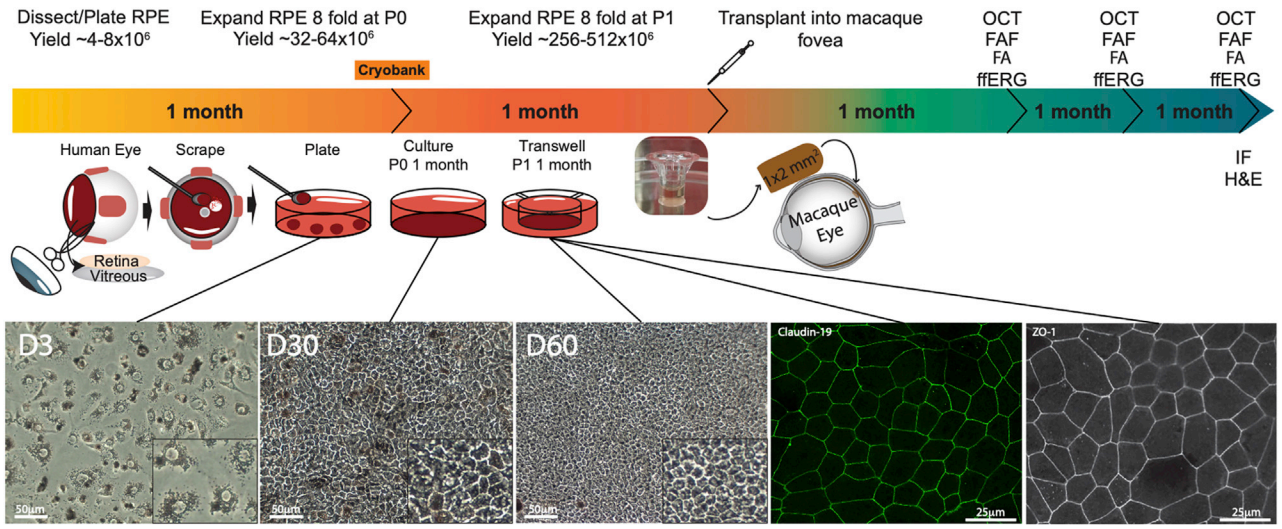

Figure 1. Diagram of hRPESC-RPE Graft Preparation, Transplantation, and *In Vivo* Follow-up in NHPs

RPE was dissected from adult cadaver donor globes and cultured for 1 month and then either replated onto transwells or cryopreserved. One month later, cultured hRPESC-RPE cells were trephined out in a 1 × 2 mm bullet shape and subretinally transplanted in the macaque macula. Optical coherence tomography (OCT), fundus autofluorescence imaging (FAF), fluorescein angiography (FA), and full-field electroretinography (ffERG) were conducted monthly. Immunostaining was conducted at 3 months.

subpopulation of RPE that exhibits stem cell characteristics has been previously characterized and termed RPE stem cell (Salero et al., 2012). Over 100,000 eyes are donated annually in the United States alone, and an average of 500 million stem cell-derived RPE cells with native physiology can be derived from each globe (Blenkinsop et al., 2015; Fernandes et al., 2018). Moreover, independent of these traits, since the cell source that will become the most successful in treating patients is yet to be established, all potential sources merit exploration. Therefore, similar to the concept of cord blood transplants, hRPESC-RPE banks could be established to provide HLA-matched RPE cells for each patient to reduce the chance of immune rejection. Subretinal injection of an hRPESC-RPE suspension has been demonstrated to rescue vision in Royal College of Surgeons (RCS) rats (Davis et al., 2017), and the cells survive and maintain their apicobasal polarity in the rabbit retina (Stanzel et al., 2014). These studies support the hypothesis that hRPESC-RPE cells are able to function *in vivo* post-transplantation and are therefore a potential alternative RPE source for cell replacement therapy.

The present study further evaluates the safety and survival of hRPESC-RPE monolayers on a polyethylene terephthalate (PET) cell carrier in a foveate non-human primate (NHP) model. This represents the first evaluation of hRPESC-RPE produced using a protocol, developed with the New York Eye Bank for Sight Restoration, seeking to establish banks of HLA-characterized RPE (Fernandes et al., 2018). The biostable PET scaffold has previously been successfully implanted in clinical trials using hESC-RPE (da Cruz et al., 2018). The study further addresses whether an hRPESC-RPE xenograft monolayer is able to maintain apicobasal polarity and support retinal function with appropriate immunosuppression and evaluate whether it has a reduced propensity to undergo epithelial-mesenchymal transition (EMT) to form epiretinal membranes (ERMs).

RESULTS

hRPESC-RPE Cell Culture

It has been demonstrated previously that hRPESC-RPE cells are derived from a subpopulation that exhibits stem cell characteristics, including the ability to divide extensively, self-renew, and differentiate into multiple progeny (Salero et al., 2012). hRPESC-RPE cells were cultured and imaged at initial plating, 1 month after initial plating, and 1 month after second plating and characterized for physiologic markers of RPE tight-junction proteins (Figure 1), similar to previous report (Fernandes et al., 2018). In addition, the heterogeneous nature of hRPESC-RPE was further examined. To ascertain the percentage of RPE capable of regenerating an RPE monolayer, a clonal analysis experiment of hRPESC-RPE was performed. Approximately 10% of the cells proliferated at least once, while only 2% of the cells were capable of re-establishing a cobblestone monolayer (n = 300 cells, n = 3 biological replicates) (Figure S1). A time-lapse video of primary RPE (n = 3 biological replicates) illustrates the RPE heterogeneity and the presence of a single cell that ultimately expands, taking over 90% of the cell culture

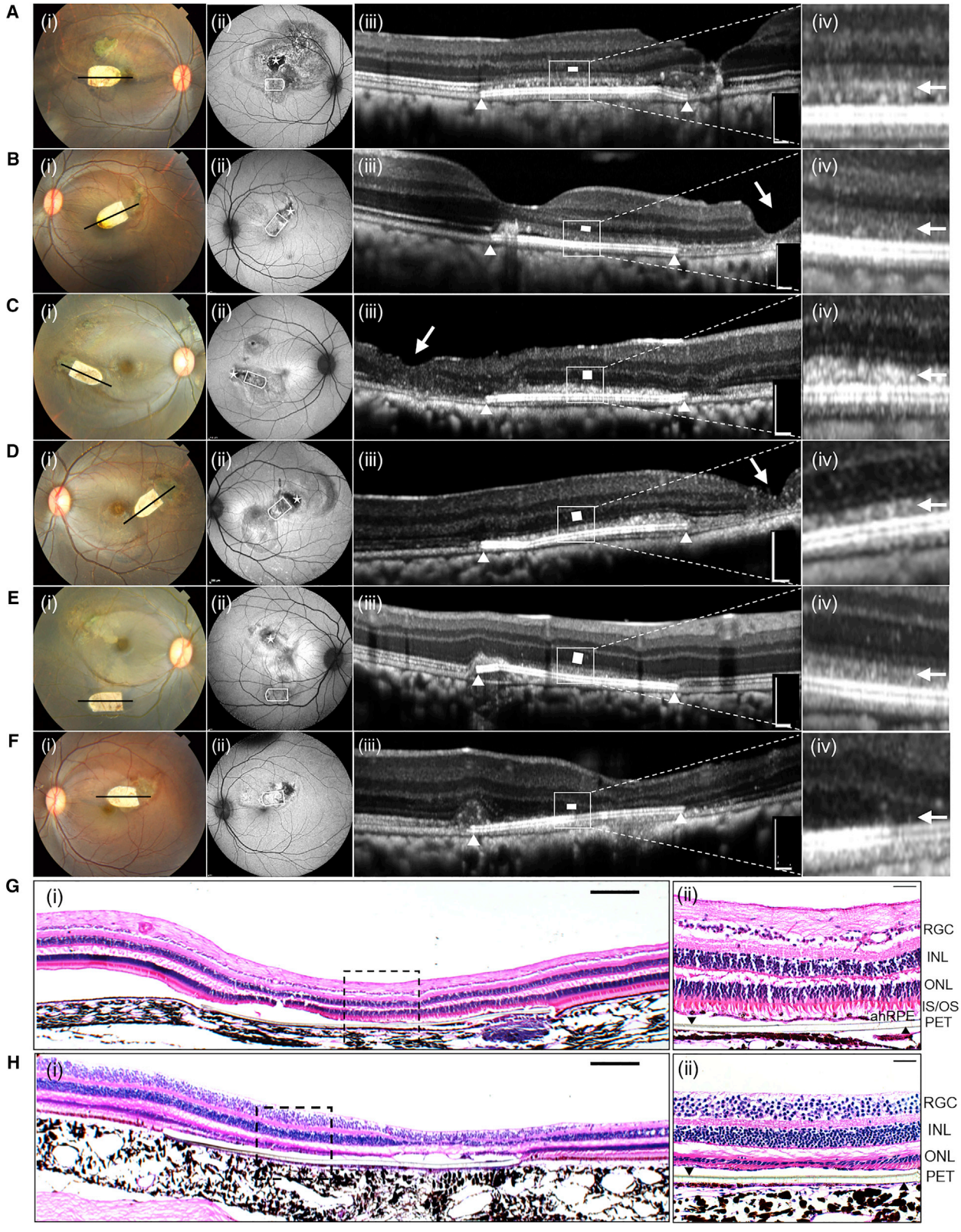

(legend on next page)

population (Video S1). These data, in addition to previously published evidence, suggest a cell in the human RPE monolayer that possesses stem cell-like characteristics, termed a human RPE stem cell. The RPE monolayers transplanted in NHPs are differentiated using the same culture.

Surgical Transplantation of hRPESC-RPE Monolayers into NHPs with Immunosuppression

Based upon close monitoring of food and drink intake, body weight, and other general signs of well-being, the systemic immunosuppression regimens were well tolerated by all NHPs. Trough levels of sirolimus were 10.4 ± 5.54 μg L^{-1} (mean ± SD, range from 8.1 to 17.2 μg L^{-1}) prior to transplantation and maintained throughout the study.

The surgical procedure of the subretinal transplantation of hRPESC-RPE monolayers on PET scaffolds is shown in Video S2. The PET scaffolds without cells (n = 2) and bleb retinal detachment (bRD) without implantation (sham, n = 2) acted as experimental controls (Table S1). The hRPESC-RPE grafts were also monitored non-invasively by *in vivo* ophthalmic assessments, identical to current human clinical practice (Figure 1, experimental diagram).

At 3 months post-implantation, all the implants remained at the site of original placement within the macula (Figures 2 and S2 and Table S1), except for case 5, wherein a large bleb was created during the surgery and the implant was displaced inferiorly post-operation (Figure 2E). Five of the seven hRPESC-RPE grafts demonstrated preservation of the outer nuclear layer (ONL) and external limiting membrane (ELM) overlying the scaffold as revealed by optical coherence tomography (OCT). In addition, fluorescein angiography (FA) images showed no vascular leakage in either early or late phases (Figure S3). In all five cases, the overlying retina was compact, with an intact ELM and ellipsoid zone (EZ) at 3 months (Figures 2A–2E). This is in contrast to PET scaffold alone (Figure 2F), where there was a loss of EZ in the overlying retina.

Transplanted hRPESC-RPE Monolayer Analysis by OCT and Histology

In a non-operated normal retina, three distinctive hyperreflective lines composed of EZ, interdigitation zone, and RPE can usually be identified on OCT (Figure 2E[iii]). However, in all hRPESC-RPE-transplanted eyes, these three otherwise distinct hyperreflective lines merge to reflect a single hyperreflective band over the scaffold, continuous with the surrounding EZ (Figure 2A–2E). However, the emitted stray light may distort the reflectance signals immediately above the implant as the PET scaffold is highly reflective. This hyperreflective band may reflect the apposition zone between transplanted RPE and endogenous photoreceptors as evidenced by the histological data (Figure 2G), where the transplanted RPE meets the endogenous photoreceptor outer segments (POSs). This new apposition zone appears as a single, hyperreflective band on OCT. Histologic processing may alter retinal adhesion, thereby producing an artifactual separation of the RPE and photoreceptor complex, or the PET carrier (e.g., Figure 2H). Notably, variations in surgical techniques contributed to RPE dysfunction localized to the site of bleb induction as indicated by hypo- and hyperautofluorescence changes on fundus autofluorescence (FAF), which ranged from mild (Figure 2B[ii]) to severe (Figure 2A[ii]). The process of denuding native submacular RPE intraoperatively prior to hRPESC-RPE introduction also contributed to localized areas of hypoautofluorescence (Figure 2A[ii] to E[ii]). The extent of FAF change does not seem to affect the eventual engraftment and integration of hRPESC-RPE with the host retina (compare Figure 2A[iii]–2E[iii]).

Changes in Retinal Layer Reflectivity Due to Intraoperative Complications

The fovea is prone to formation of a macular hole during surgical bleb formation; OCT scans obtained across the fovea over a period of 3 months confirmed that ONL thickness and EZ were preserved in successful surgery (Figure 3).

Figure 2. Fundus Photographs, OCT, and Histology of NHP Eyes 3 Months after submacular Transplantation of hRPESC-RPE Grafts

(A–F) Five NHPs (A–E) received hRPESC-RPE monolayer transplantation without major surgical complications. (F) One implantation case of PET scaffold alone. Column (i): color fundus photographs showing white bullet-shaped implants subretinally at 3 months. Column (ii): FAF imaging at 3 months. White bullet shape indicates the final location of hRPESC-RPE implants; asterisk indicates the location at which the NHP RPE is surgically removed prior to the transplantation. Column (iii): OCT images were taken through the midline of the bullet-shaped implants as indicated by black lines in column (i). White triangles indicate the limit of the implants in the subretinal space. Single white arrow indicates the site of retinotomy (surgical incision) (B[iii], C[iii], and D[iii], where localized full-thickness retinal atrophy has occurred at 3 months). White rectangles indicate the ONL. White triangles indicate the limit of the RPE grafts. Column (iv): higher-magnification OCT image of the outer retina just above the implant. A hyperreflective band, continuous with the ellipsoid zone, is seen here as indicated by a white arrow. This hyperreflective band likely reflects the integration zone between transplanted RPE and endogenous photoreceptors. There was no evidence of epiretinal membrane formation in any of the cases.

(G) H&E staining indicating preserved retinal structure above area of hRPESC-RPE transplant.

(H) H&E staining indicating ONL thinning and outer segment (OS) lost above the area of PET alone. Scale bars, 200 μm in column (iii) and 100 μm in (G) and (H). INL, inner nuclear layer; IS, inner segment; RGC, retinal ganglion cell layer.

See also Figures S1 and S2.

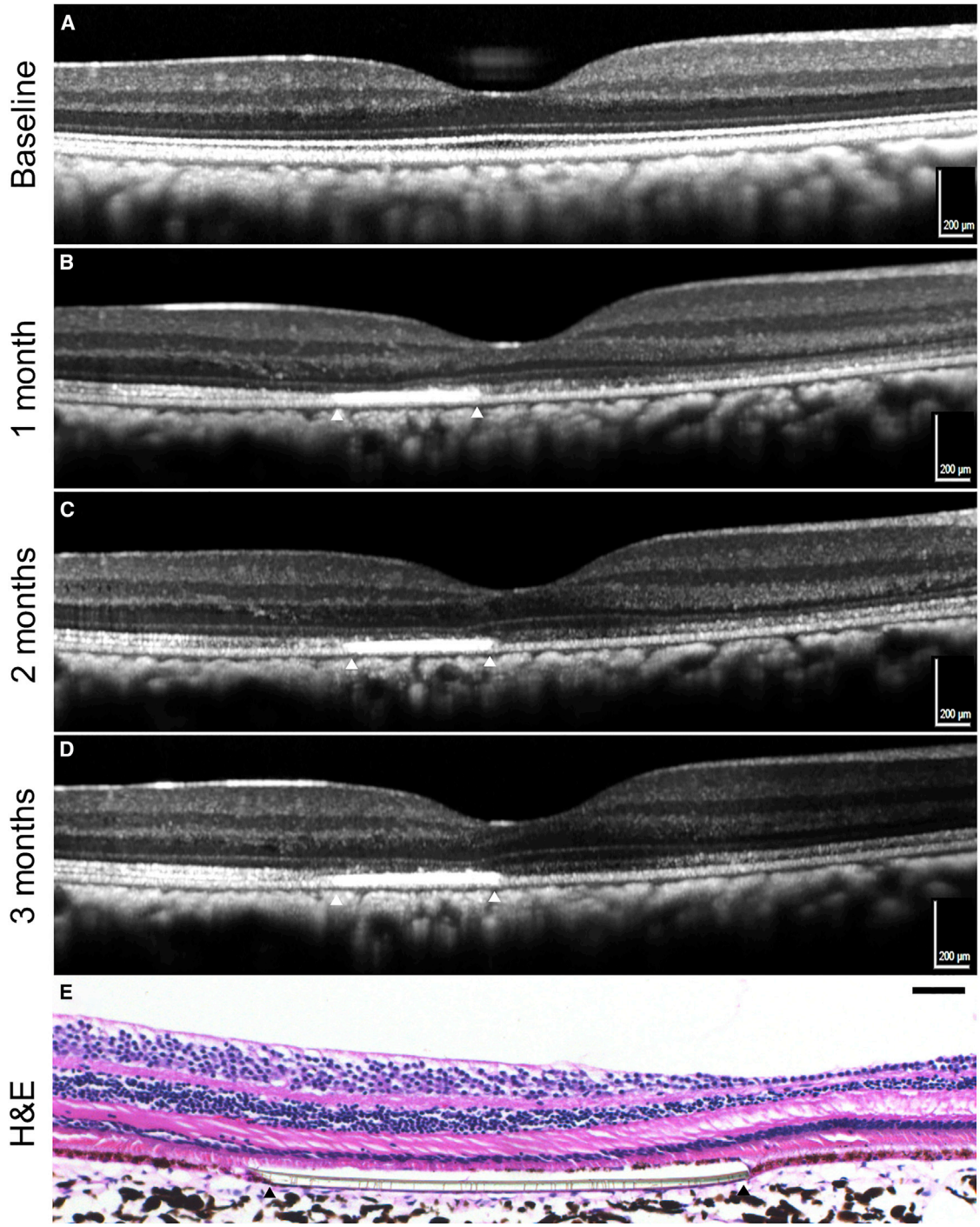

Figure 3. OCT Tracking Scans and Histological Image of Submacular-Transplanted hRPESC-RPE Graft in a Single NHP

(A–D) OCT scans were obtained across the center of fovea over a period of 3 months. White triangles indicate the lateral extremes of the subretinal implants. Note the preserved ONL thickness overlying the transplant, compared with the nasal macular region. The ellipsoid zone is less discernible and thinner over the implant, while hyperreflective dots are seen in the nasal macula. (A) Baseline, (B) 1 month, (C) 2 months, (D) 3 months.

(E) H&E image indicating presence of hRPESC-RPE and PET scaffold, with well-preserved ONL overlying the RPE graft. Scale bars, 200 µm in (A–D), 50 µm in (E).

See also Figure S1.

Surgical complications may result in retinal atrophy of the overlying retina post-transplantation. Of the seven cases, there was one instance of retinal trauma and one of subretinal hemorrhage. Retinal injury occurred during the initiation of retinal bleb with a 38 G needle (case 7). At 1 week post-surgery, a loss of retinal structure was observed, with increased hyperreflectivity throughout all retinal layers on OCT. This progressed to severe retinal atrophy by 1 month (Figure S2A). In contrast, immune-mediated ONL loss progresses at a much slower rate (Diniz et al., 2013). This highlights the importance of detailed surgical documentation, as surgically induced trauma may be mistaken for graft rejection. Fortunately, not all intraoperative complications led to a poor outcome in hRPESC-RPE engraftment. The subretinal hemorrhage (approximately 3 discs in diameter) that occurred in case 6 had almost resolved in 1 month, with only minimal subretinal fluid at 3 months. This indicates tolerance and engraftment of the hRPESC-RPE graft despite the presence of subretinal hemorrhage. Moreover, OCT showed preservation of ONL thickness and ELM overlying the hRPESC-RPE graft (Figure S2B). In addition, in sham controls where retinal blebs were raised but neither scaffold nor cells implanted, retinal structure was maintained, with retinal atrophy limited to the site of retinotomy after 1 month (Figure S2C).

Measurement of ONL Thickness in Retina Overlying Transplanted hRPESC-RPE Graft

Preservation of ONL thickness over time was studied as a surrogate marker for hRPESC-RPE engraftment; this assumes that functional RPE is required for photoreceptor preservation. ONL thickness measurements based on OCT volume scans were performed at 1 month for RPE grafts (n = 5), scaffold alone (n = 2), and sham retinal detachment (n = 2) (Figure 4). The results show that average ONL thickness over the area of transplant was 39.860 ± 0.014 μm (mean ± SEM) at 1 month and maintained at 3 months (39.519 ± 0.019 μm, p = 0.9326). This was thicker than scaffold alone without cells at 1 month (35.559 ± 0.020 μm, $p < 0.0001$), but thinner than both non-transplanted (reference) and sham retinal detachment (51.386 ± 0.014 μm, $p < 0.0001$, and 48.650 ± 0.011 μm, $p < 0.0001$, respectively).

Expression of RPE-specific and POS Phagocytosis Markers by Transplanted hRPESC-RPE

Post-transplantation, the survival of hRPESC-RPE grafts at 3 months was supported by the presence of hRPESC-RPE cells stained with human-specific markers STEM121 and TRA-1-85 (Figure 5B and 5D), absent in native NHP RPE (Figure 6F). Importantly, there were neither signs of apoptosis, as indicated by the absence of cleaved caspase-3 (Figure S4B), nor continued proliferation, as indicated by the absence of Ki67 (Figure S4A). Thereafter, it was important to ascertain whether the hRPESC-RPE continued to recover RPE-specific markers (RPE65 and CRALBP) *in vivo* and, if so, whether the cells were functional. In hRPESC-RPE grafts, there was a noticeable increase in expression of both RPE65 (Figure 5D) and CRALBP (Figure 5F) at 3 months post-transplantation compared with pre-transplanted cultures (Figures 5C and 5E, respectively). Expression of OTX2, a homeobox gene important for function of the RPE (Bovolenta et al., 1997) and present in pre-transplanted RPE (Figure 5E), was also maintained post-transplantation (Figure 5F). To demonstrate additional hRPESC-RPE functionality, phagocytosis was assessed by co-staining with the apical RPE marker ezrin and the POS marker rhodopsin. Rhodopsin-positive puncta were observed underneath the apical membrane of hRPESC-RPE, suggesting outer segment phagocytosis and processing (Figure 5G).

Expression of Key Epithelial-Mesenchymal Transition Markers in the hRPESC-RPE Monolayer

Post-retinal surgery, the RPE may undergo EMT that leads to either ERMs or proliferative vitreoretinopathy (PVR) (Charteris, 1995). RPE cells in culture express αSMA if they are not fully differentiated or on the verge of EMT. hRPESC-RPE did not express EMT markers such as COL1A1 and αSMA either pre-transplantation (Figure 6A) or at 3 months post-transplantation (Figure 6B). Vimentin protects cells against nuclear rupture and DNA damage during migration and is another marker for EMT (Patteson et al., 2019). As the hRPESC-RPE cells were cultured for only about 4 weeks, it was considered that vimentin may still be present but may be downregulated after 3 months *in vivo*. As predicted, pre-transplanted RPE did exhibit vimentin (Figure 6D), but at 3 months post-transplantation, the expression of vimentin was reduced (Figure 6E). To evaluate the inflammatory status of the transplanted region, the overlying retina was examined for evidence of retinal gliosis. The presence of hRPESC-RPE did not induce localized retinal gliosis, as indicated by the reduction of both vimentin and glial fibrillary acidic protein (GFAP) (Figure 6H) compared with the PET scaffold alone (Figure 6G) and sham retinal detachment (Figure 6I).

Full-field Electroretinography Measurement Post hRPESC-RPE Transplantation

The potential toxicity and impact on global retinal function of the retinal graft transplantation of hRPESC-RPE was assessed by full-field electroretinography (ERG). There was no significant effect on ERG amplitudes or timing under either dark-adapted or light-adapted conditions

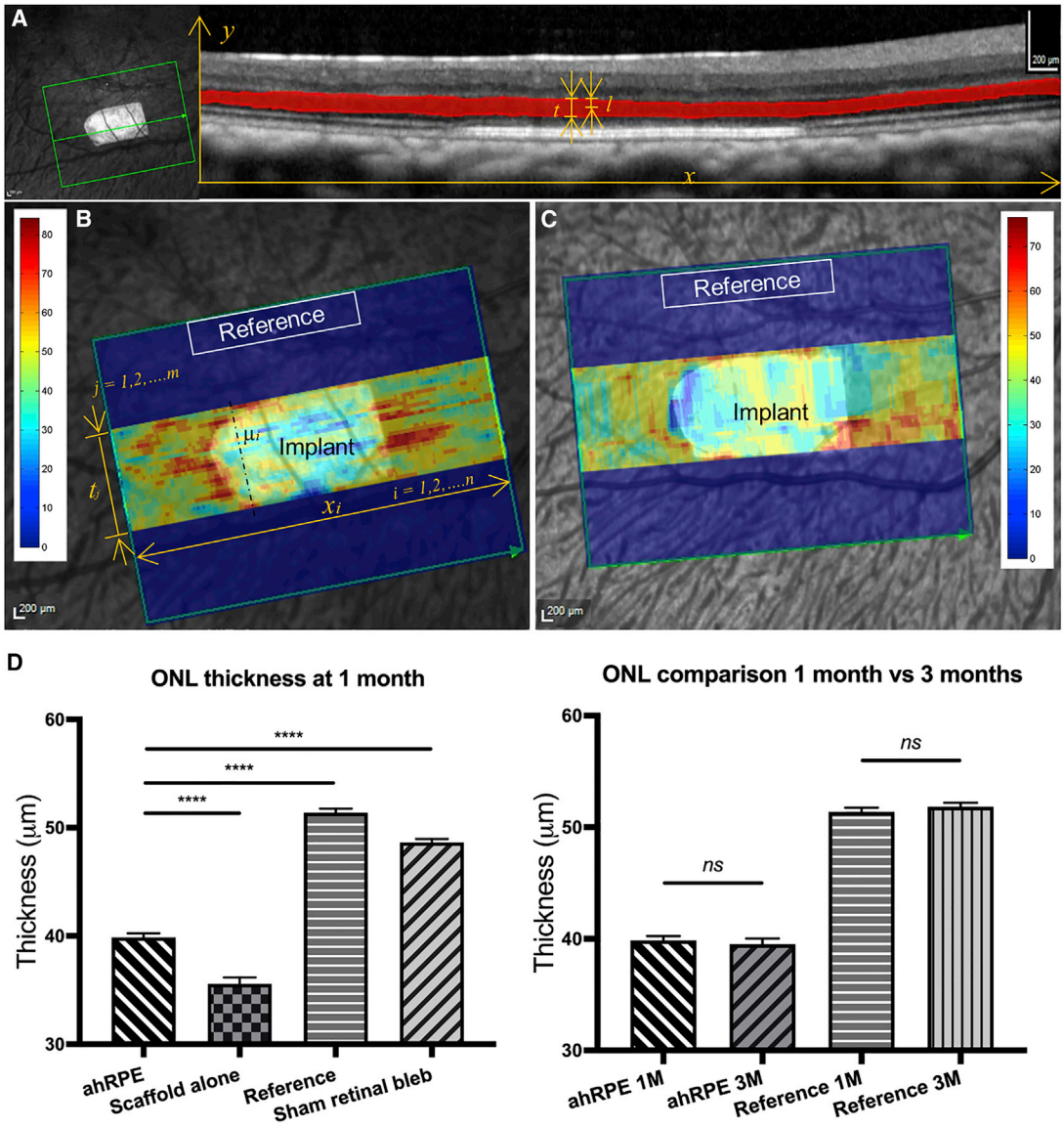

Figure 4. ONL Thickness Measurements at 1 and 3 Months Post-Transplantation

(A) Image of OCT volume scan. Left: confocal scanning laser ophthalmoscope (cSLO) image; green box indicates scanned region, with bullet-shaped implant in the center. Green arrow indicates position at which an individual OCT scan was taken, which is displayed at the right. The ONL was manually outlined and highlighted in red on OCT images (right). The symbol *l* presents the shortest length between the annotated layer's edge and the middle line along the y-axis and *t* is the measured ONL thickness.

(B and C) Heatmaps superimposed on an en face cSLO image of a transplanted hRPESC-RPE graft taken at 1 month (B) and 3 months (C) *in vivo*. ONL thickness measurements were performed in two zones, termed "Implant" and "Reference," respectively. In B, *m* indicates the total number of z-stack images, and *n* indicates the width along *x*-axis.

(D) ONL thickness comparison of the RPE grafts (ahRPE) in (B) and (C), reference regions, PET scaffold alone, and sham retinal detachment. The data are presented as mean ± SEM. Statistical analysis was performed using ANOVA with Tukey *post hoc* test. The average ONL thickness over the transplanted RPE was maintained at 39.860 ± 0.014 µm at 1 month, with no change to 39.519 ± 0.019 µm at 3 months, thinner than the ONL thickness at the reference area (51.386 ± 0.014 µm, ****$p < 0.0001$) and sham surgery (48.650 ± 0.011 µm, ****$p < 0.0001$), but thicker than those above PET without cells (35.559 ± 0.020 µm, ****$p < 0.0001$) at 1 month. Scale bars, 200 µm in (A–C). *ns*, not significant.

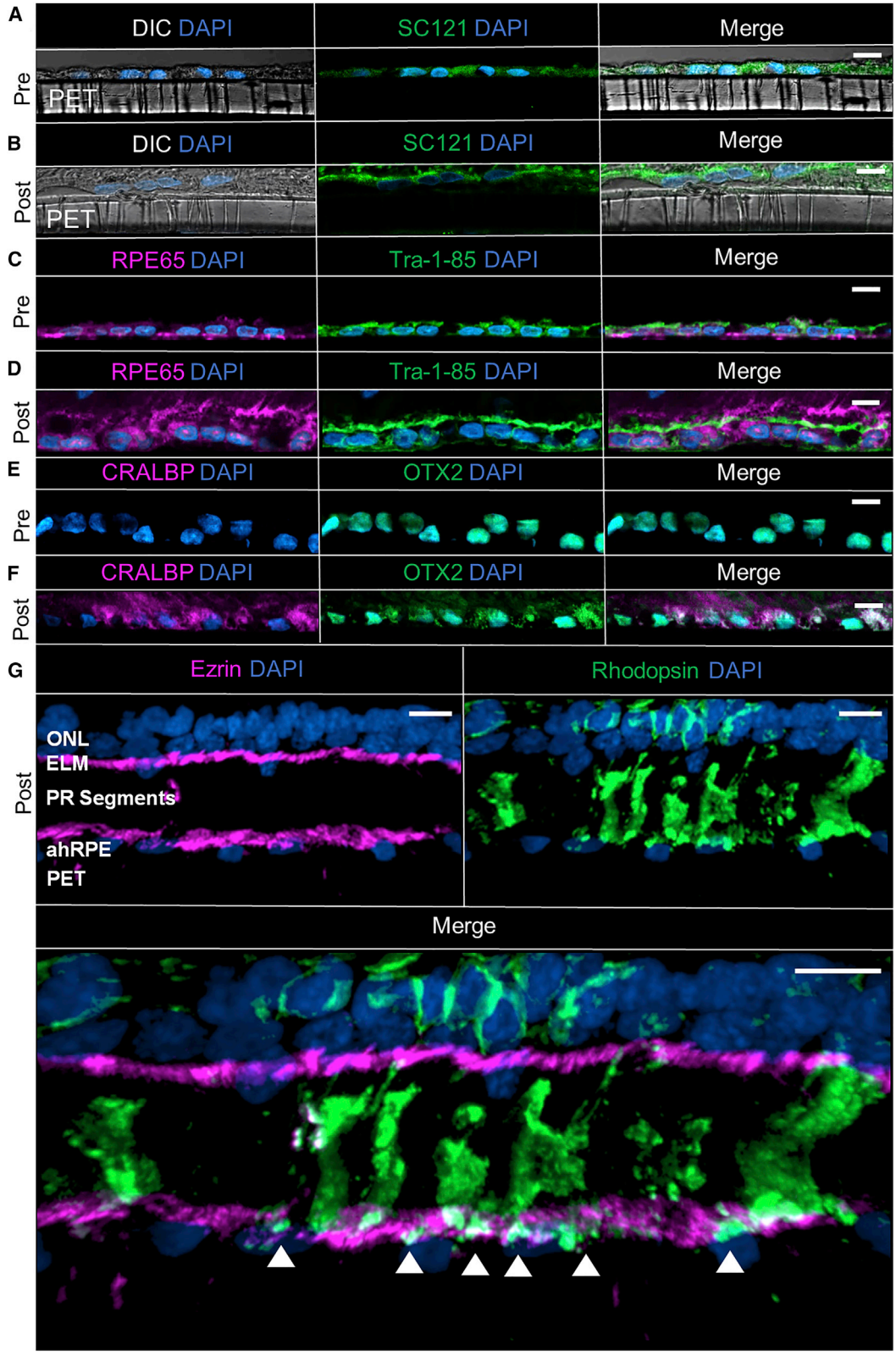

(legend on next page)

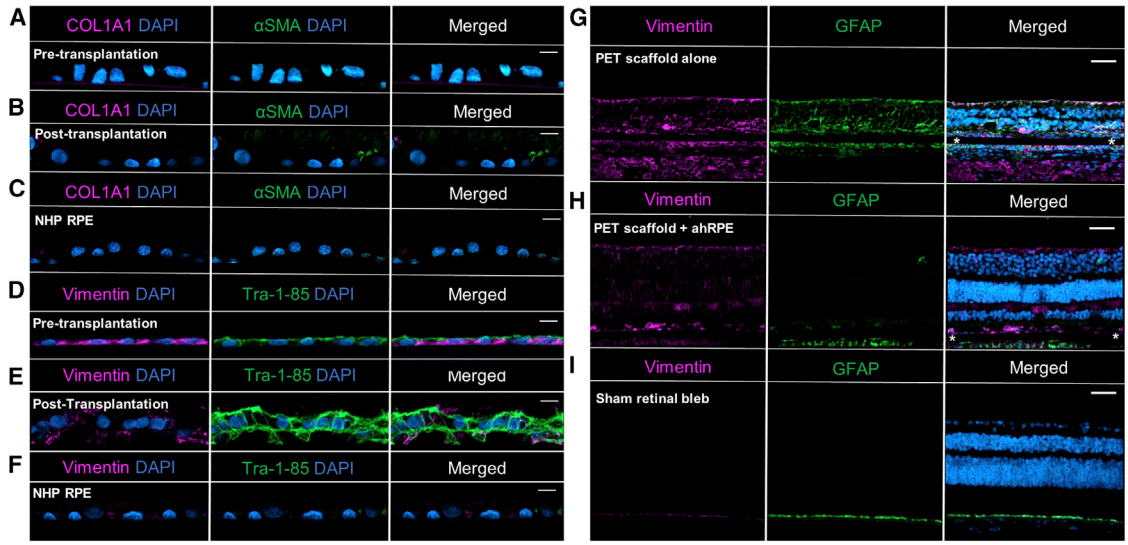

Figure 6. Matured hRPESC-RPE *In Vivo* Suppresses Gliosis in Adjacent Retina and Does Not Express Characteristic Markers of EMT

Expression of the classical EMT markers COL1A1 and αSMA was absent both (A) pre- and (B) post-transplantation of hRPESC-RPE on PET at 3 months.

(C) Adjacent native NHP RPE also did not express either EMT marker.

(D) Pre-transplanted RPE, marked with the human-specific marker TRA-1-85, expresses vimentin.

(E) At 3 months, vimentin expression is present but downregulated in TRA-1-85-positive hRPESC-RPE.

(F) Adjacent NHP RPE is negative for both vimentin and TRA-1-85.

(G) Increased expression of retinal gliosis markers vimentin and GFAP in the retina overlying transplanted PET scaffold alone (without cells).

(H) In contrast, vimentin and GFAP expression is reduced at 3 months in the overlying retina of the hRPESC-RPE graft.

(I) Absence of vimentin and GFAP expression indicated lack of gliosis in sham retinal bleb control. Asterisk indicates position of PET scaffold. Scale bars, 10 μm in (A–E) and 50 μm in (G–I).

3 months post-transplantation (Figure 7), as also the case for PET scaffold without cells (Figure S5), confirming that the global function of both rod and cone photoreceptors is maintained despite transplantation of the hRPESC-RPE. Importantly, the absence of significant deterioration was demonstrated in all seven NHPs (Figure 7).

DISCUSSION

This study addresses whether transplantation of hRPESC-RPE on PET scaffolds can successfully engraft underneath the macula of an NHP, which is of clinical importance as a cell therapy for AMD and other macular degenerations. The data demonstrate for the first time that hRPESC-RPE monolayers are stable, have a good safety profile, and are able to recover and function subretinally for at least 3 months underneath the NHP macula. These data support previous findings wherein hRPESC-RPE monolayers were preserved in rabbits (Stanzel et al., 2014) and were able to rescue vision in RCS rats (Davis et al., 2017). The transplanted hRPESC-RPE continues to recover underneath the macaque retina as shown by the enhanced expression of RPE-specific markers such as RPE65, accompanied by a

Figure 5. Functional Phagocytosis Demonstrated *In Vivo* in Transplanted hRPESC-RPE after 3 Months Maturation

(A–F) Comparison of pre-transplantation hRPESC-RPE on PET scaffold (A, C, and E), with post-transplantation hRPESC-RPE *in vivo* (B, D, and F). The differential interference contrast (DIC) microscopy images showed cells laid on the PET scaffold. STEM121 and TRA-1-85, human-specific markers, were used to confirm the presence of hRPESC-RPE cells. RPE recovery occurs *in vivo* at 3 months as indicated by the increased expression of RPE-specific markers such as RPE65 (compare D with C) and CRALBP (compare F with E). At 3 months, OTX2 expression is maintained (F compared with E).

(G) Transplanted RPE attained polarity *in vivo* as indicated by apical localization of ezrin. Transplanted RPE demonstrated functional phagocytosis by the presence of internalized rod photoreceptor outer segments stained with rhodopsin (white arrowheads) within transplanted RPE. Scale bars, 10 μm.

See also Figure S3.

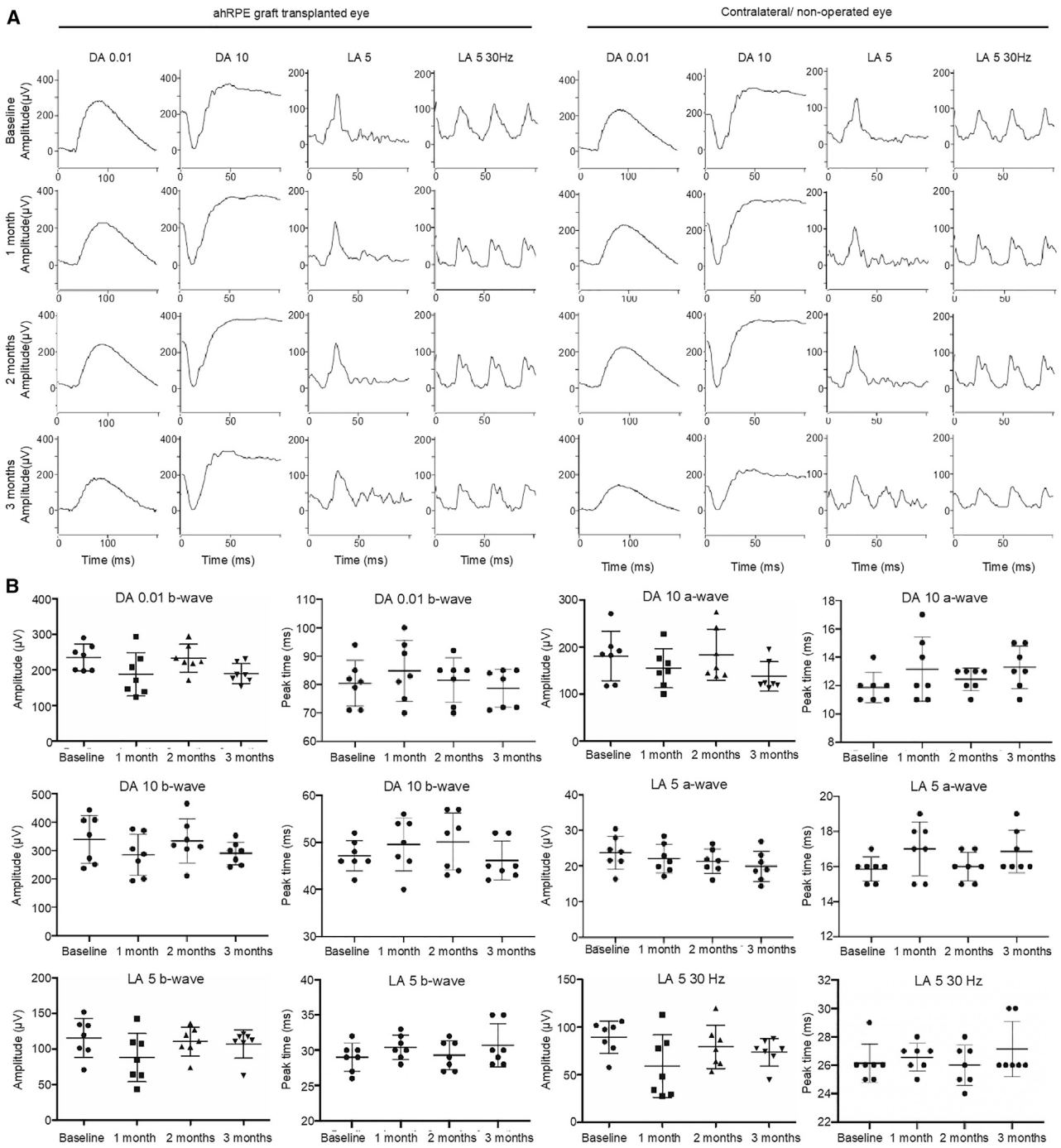

Figure 7. Functional Assessment of NHP Retina by Full-field ERG

(A) Full-field ERG showed normal waveforms in the eye with transplanted hRPESC-RPE monolayer compared with the contralateral (non-operated) eye during the 3 month follow-up.

(B) Scatterplots of amplitudes and peak times in $n = 7$ monkey eyes with transplanted RPE monolayers at baseline and 1, 2, and 3 months. There were no significant changes in waveform amplitudes and peak times between baseline and follow-ups. Data are shown as mean ± SD. Statistical analysis was performed using ANOVA with Tukey's *post hoc* test.

See also Figure S5.

downregulation of mesenchymal markers such as vimentin. This is consistent with previous studies wherein retinoid-cycle protein expression levels decreased after isolation from native tissues and recovered post-transplantation after adjustment to the environment (Maeda et al., 2013; Masuda et al., 2014; Samuel et al., 2017). The hRPESC-RPE is able to support the overlying photoreceptor by phagocytosis and maintain ONL thickness better than PET-alone controls. In addition, subretinal-transplanted hRPESC-RPE monolayers did not undergo EMT, nor were ERMs observed. Gliosis was not observed in adjacent retina. Together, these results suggest that transplantation of hRPESC-RPE is well tolerated and has potential for the treatment of RPE disease, including AMD.

The developmental state of hRPESC-RPE has been shown to contribute to vision rescue in the RCS rat (Davis et al., 2017) and to subretinal integration patterns in rabbits (Ilmarinen et al., 2019). The present study evaluated the recovery and function of the hRPESC-RPE after transplantation into NHPs. There was increased expression of RPE65 and CRALBP, in keeping with a functioning visual cycle. Maintenance of the expression of OTX2, a homeobox protein that drives expression of genes essential for RPE function, was also observed. In addition, by comparing TRA-1-85 staining, we demonstrated an increased apicobasolateral length of the hRPESC-RPE after transplantation, also suggestive of cell recovery (Fields et al., 2020; Yeaman et al., 1999). These data, in association with the absence of Ki67-positive and cleaved caspase-3 detection in the RPE, suggest that transplanted cells are neither hyperproliferating nor undergoing apoptosis, but instead processing cues from the *in vivo* environment and recovering functional expression of RPE markers. The internalization of POS is indicative of phagocytosis and further supports the functional replacement of native RPE by the transplanted hRPESC-RPE monolayer.

ERM has recently been reported following RPE transplantation (da Cruz et al., 2018) and it was therefore important that the present study evaluated markers of RPE undergoing EMT and identified changes in the maturity of RPE pre- and post-transplantation. There was a decrease in vimentin and an absence of αSMA, both markers of EMT. Combined with the phagocytosis and the absence of evidence of proliferation, these observations suggest that the RPE identity of transplanted RPE is maintained rather than undergoing EMT. An additional factor contributing to the absence of both ERM and PVR following transplantation may be the use of the RPE as a monolayer rather than suspension. This minimizes the risk of RPE reflux from the retinotomy site, a known risk factor for ERM and PVR (Charteris, 1995). Of note, the absence of both ERM and PVR in the current study contrasts with previous studies wherein ERMs were still reported (da Cruz et al., 2018) despite the use of RPE monolayers. It cannot be excluded that this may simply reflect the use of normal NHPs (i.e., non-diseased) in the present study, compared with clinical trials wherein transplants were performed underneath severely diseased retinas (da Cruz et al., 2018; Kashani et al., 2018; Mandai et al., 2017; Schwartz et al., 2015). Future experiments will endeavor to study hRPESC-RPE in an NHP model of retinal degeneration for a longer time period, thereby more closely resembling the clinical pluripotent stem cell-derived RPE transplant studies.

Full-field ERG is a long-established method to evaluate global changes in retinal function following surgical interventions such as RPE transplantation and as a surrogate marker for safety and tolerability. Reduction in ERG was previously reported by another group in two patients after hESC-RPE transplantation at 6 months, with recovery at 12 months in one patient but not the other, possibly due to re-detachment requiring a second surgery and/or presence of silicone oil (da Cruz et al., 2018). The present study found no detectable ERG changes as a result of hRPESC-RPE grafts, indicating no detrimental effect on generalized retinal function, which assisted in confirming the safety of the procedure. However, it should be noted that full-field ERG does not assess macular function specifically, and future studies should evaluate function in the transplanted area using multi-focal or pattern ERG.

There are several limitations of this study. First, in the absence of an ideal disease model, subretinal transplant of hRPESC-RPE monolayers was performed in normal NHPs with prior denudation of RPE (performed in a single surgery). Host RPE denudation and subretinal transplant of RPE cannot be performed in two separate surgeries, as extensive subretinal fibrosis would prevent subsequent raising of the subretinal blebs required for RPE transplantation. Similar observations are available from a clinical trial with hESC-RPE monolayer grafts in AMD (GA) (Kashani et al., 2020). Future studies will attempt to study rescue in a laser-induced dystrophic RPE model with diseased Bruch's membrane (Sharma et al., 2019) to gauge a possible therapeutic benefit. In addition, variability in hRPESC-RPE pigmentation overlying the implant is observed. RPE cells are known to divide their pigment granules as they divide and under some conditions will resynthesize pigmentation. However, the regulation of RPE pigmentation is still not entirely understood. Strong pigmentation noted at the tip of the bullet-shaped implants (Figures 2A [i] and 2B[i]) may be due to the denudation of native RPE in the process of inserting the hRPESC-RPE monolayer implant.

A second limitation of this study is that it is a xenotransplant. This possibly limits the subretinal integration of hRPESC-RPE due to both systemic and local immune reactions (Stanzel et al., 2014, 2019). Similar to our observation

of reduced ONL underneath the xenografted RPE monolayer, Diniz et al. also observed progressive reductions in athymic nude rats receiving hESC-RPE transplants, suggesting a variant of a graft-versus-host reaction (Diniz et al., 2013). Furthermore, as a feasibility-only study utilizing non-GMP (good manufacturing processes)-grade hRPESC-RPE monolayer xenotransplants, the present study is likely to underestimate efficacy compared with the mandatory use of GMP-grade hRPESC-RPE cell therapeutics in human clinical trials (da Cruz et al., 2018; Kashani et al., 2018; Mandai et al., 2017; Schwartz et al., 2015). In addition, the use of systemic immunosuppression further limits the interpretation of present data, in particular, the lack of ERMs or PVR observed in NHPs. Future clinical trials involving hRPESC-RPE could include HLA matching, as used in recent iPSC-RPE allogeneic transplantation with HLA-matched, major histocompatibility complex-homozygous RPE, and might possibly remove the need for systemic immunosuppression (Sugita et al., 2020). Last, the hRPESC-RPE transplants were followed up for 3 months. The long-term (beyond 3 months) survival of hRPESC-RPE xenografted in NHPs is unclear, albeit that the present study was not designed primarily to assess RPE survival. However, in the context of treating AMD, wherein long-term RPE function is required, strategies such as HLA matching and appropriate patient selection will play key roles in long-term graft function.

In conclusion, subretinal transplantation of an hRPESC-RPE monolayer can be performed safely under the macula of a healthy NHP model and survives for at least 3 months in the presence of systemic immunosuppression. The data suggest that the hRPESC-RPE graft recovers cellular functions such those involved in the visual cycle, the maintenance of polarity, and photoreceptor phagocytosis. The lack of any suggestion of deleterious effects encourages optimism that hRPESC-RPE may become a promising alternative source of RPE for cell replacement therapy for patients with RPE-dysfunction-related vision loss.

EXPERIMENTAL PROCEDURES

hRPESC-RPE Culture

Human globes from donors ages 69 and 81 years were obtained from the Eye-Bank for Sight Restoration (New York, NY) and Miracles in Sight (Winston-Salem, NC). Neither ethics approval nor consent was needed for the utilization of donor tissue. This was confirmed with the institutional review board of the Program for the Protection of Human Subjects, Icahn School of Medicine at Mount Sinai. Donors died of lung cancer and myocardial infarction and were negative for all tested serology. A detailed protocol on isolation and characterization of RPE used for this study has been previously published (Blenkinsop et al., 2013; Fernandes et al., 2018). Briefly, globes were obtained within 24 h of death. RPE cells were digested with trypsin intraocularly for 50 min. They were then brushed off Bruch's membrane, collected, and plated on tissue culture plates coated with 10 μg mL^{-1} Synthemax II (Corning, USA) in RPE medium (Blenkinsop et al., 2013) containing DMEM/F12 (Gibco), supplemented with 10% heat-inactivated fetal bovine serum (FBS, Sigma), 1× GlutaMAX (Gibco), 1× MEM non-essential amino acids solution (Gibco), 1× penicillin-streptomycin (10,000 U mL^{-1}, Gibco), 1× sodium pyruvate (100 mM, Gibco), and 10 mM nicotinamide (Sigma-Aldrich), which was changed three times a week. After the first week, FBS was reduced to 2%. Cultured hRPESC-RPE (passage 1) on inserts (PET, Millipore) were maintained for 3 weeks before transport from the United States to Singapore (Stanzel et al., 2014). Once received, the cells were further cultured for 1 to 2 weeks before transplantation.

A passage 0 human RPE cobblestone culture was scraped in the center of the RPE monolayer, trypsinized, and replated clonally into 1 mm^2 Terasaki plates. Images of the cells were taken at regular time points. The ability of these cells to clonally divide was quantified, as was the ability of the cells to re-establish a cobblestone monolayer. The same passage 0 RPE cobblestone culture was scraped, trypsinized, and replated at 5,000 cells cm^{-2} and time-lapse imaging was performed every 30 min for 12 days.

Animals

Nine cynomolgus monkeys (*Macaca fascicularis*) weighing 3.0–5.0 kg (4–6 years old, four males and five females) were sourced from SingHealth Experimental Medicine Center, Singapore. All animal studies were approved by the institutional animal care and use committee of SingHealth, Singapore (2015/SHS/1092). All experiments and animal care procedures were in accordance with the Association for Research in Vision and Ophthalmology's *Statement for the Use of Animals in Ophthalmic and Vision Research* and performed in an AAALAC International-approved facility.

Immunosuppression

All NHPs received systemic immunosuppression 7 days prior to and throughout the experiments (3 months post-surgery). Sirolimus was used orally with a loading dose of 2 mg, followed by a 1 mg daily dose. Tetracycline antibiotics (doxycycline and minocycline) were administered orally in doses of 7.5 mg kg^{-1} body weight (BW), twice a day as previously described (Sharma et al., 2019; Stanzel et al., 2019). All animals were monitored closely to ensure that the immunosuppression had no effect on the general well-being of the animals. Significant body weight loss (more than 10%), loss and/or decrease in appetite or water consumption, ungroomed hair loss, abnormal aggression, and reluctance to move, any of which would suggest an undesired effect on well-being, were monitored by an independent senior veterinarian, and none were observed in any animal for the duration of the study. Sirolimus levels in blood were tested on the day of surgery, at 3 weeks, and at 3 months post-surgery by liquid chromatography-tandem mass spectrometry (Singapore General Hospital Biochemistry Laboratory).

Animal Surgery

hRPESC-RPE patch transplantations were performed on NHPs under general anesthesia (Liu et al., 2019; Stanzel et al., 2019). In

brief, induction of anesthesia was done using atropine (0.05 mg kg^{-1} BW) and ketamine (10 mg kg^{-1} BW) and general anesthesia was induced with 2% isoflurane and maintained with 0.5%–2% isoflurane. A three-port, 25 G vitrectomy was performed using chandelier illumination. Posterior vitreous detachment was induced and assisted by triamcinolone and 25 G intraocular forceps. A 38 G cannula (MedOne Surgical, USA) was used to create a bRD by manually injecting balanced salt solution into the macular area. The retinotomy was enlarged with vertical vitreous scissors (Alcon, USA). One sclerotomy was extended to admit 20 G instrumentation. The host submacular RPE was scraped prior to implantation of hRPESC-RPE with a 20 G custom extensible loop instrument (Thieltges et al., 2016) to prevent the host RPE from acting as an additional barrier between the host choriocapillaris and the transplanted RPE.

Bullet-shaped hRPESC-RPE grafts ($n = 7$) were inserted subretinally using a custom-made device (Al-Nawaiseh et al., 2016; Liu et al., 2014; Stanzel et al., 2012). Implantation of a PET membrane without cells ($n = 2$) and sham retinal bleb without implantation ($n = 2$) served as controls. Fluid-air exchange was performed to reattach the retina. Microscope-integrated intraoperative OCT was used to guide the surgery. Preservative-free triamcinolone (0.05 mL of 40 mg mL^{-1}) was injected intravitreally at the end of the surgery. The sclerotomy and conjunctiva were sutured with 7-0 vicryl sutures. A topical antibiotic and steroid ointment (Tobradex, tobramycin and dexamethasone, Alcon, USA) and homatropine eye drops were applied to the treated eyes twice a day for 5 days post-surgery.

In Vivo Animal Follow-up

The subsequent clinical course of the submacular hRPESC-RPE grafts was monitored non-invasively by ophthalmic imaging devices at 3, 7, and 14 days post-surgery and then monthly for 3 months. OCT was performed using a Heidelberg Spectralis (Heidelberg Engineering, Germany), which provides *in vivo* depth image and layer-specific information of the retina with eye-tracking capabilities. It also allows the OCT scans to be obtained at the same position at baseline and on follow-up examinations. Scanning laser ophthalmoscope-based FAF and retinal FA were also obtained using the same device; color fundus images were taken by a fundus camera (Zeiss, Germany).

Retinal function was assessed by ERG using an Espion system (Diagnosys, USA) with protocols and procedures based upon those recommended for humans by the International Society for Clinical Electrophysiology of Vision, but with an LA 5.0 stimulus strength (McCulloch et al., 2015).

Outer Nuclear Layer Measurement Based on OCT Volume Scan

Computation of the ONL thickness was based on OCT volume scans of hRPESC-RPE grafts ($n = 5$) at 1 and 3 months and of scaffold alone ($n = 2$) or sham retinal bleb ($n = 2$) at 1 month. The thickness analyses were initially annotated by a masked grader. The manual annotation process was conducted using a segmentation editor plug-in tool in ImageJ software package (Wayne Rasband, National Institutes of Health, USA), as shown in Figure 4A. Two regions, "Implant" (retina directly above the implant) and "Reference" (healthy retina adjacent to the implant), were considered for analysis. All annotated images were further calculated using MATLAB software package (MATLAB, Math Works).

The measured ONL thickness (t) is calculated by Equation 1, where l presents the shortest length between the annotated layer's edge and the middle line along the y axis in Figure 4A:

$$t = 2 \times l. \quad \text{(Equation 1)}$$

Subsequently, the sum of thickness (z) is calculated from t as shown in Equation 2 and the mean thickness μ_i at i position of x across the z stack images is computed with Equation 3:

$$z = \sum_{j=1}^{m} t_j \quad j = 1, 2, \ldots\ldots m, \quad \text{(Equation 2)}$$

$$\mu_i = \frac{z_i}{n} \quad i = 1, 2, \ldots . n, \quad \text{(Equation 3)}$$

where m indicates the total number of z stack images, and n indicates the width along the x axis. A 3D reconstruction video of the volume above the bullet-shaped implant was generated (Video S3).

Histopathological Examination

All animals were euthanized (Table S1) with perfusion fixation using 10% formalin while in deep intramuscular anesthesia. Thereafter, the entire eye globes were enucleated and immersed in 10% formalin for another 24 h at 4°C. Tissue samples (retina-sclera) were cut with a surgical blade (approximate 3 × 2 mm, area 6 cm^2) to ensure full coverage of the transplanted RPE graft (2.2 × 1.1 mm, area 2.42 cm^2) and embedded in paraffin. Approximately 50%–70% of the graft area was sectioned into 10 μm thick slices with a microtome (Leica RM2255, Germany), with three retina slices on each slide. At least five slides, regularly spaced from one another, were used for H&E staining for histological analysis. A total of 5 slides × 3 sections = 15 retinal slices were sampled. Light micrographs were taken on a Nikon Eclipse Ti microscope equipped with a digital camera.

Immunostaining of Tissue Sections

Paraffin-embedded sections were deparaffinized in two xylene immersions followed by rehydration through a graded ethanol series of decreasing concentrations. The slides were subjected to antigen retrieval using sodium citrate buffer (pH 7) and allowed to cool to room temperature (RT) before immunostaining. Slides were blocked for 1 h at RT and then incubated with primary antibodies overnight at 4°C and secondary antibodies for 1 h at RT (Table S2). Nuclei were stained with Hoechst 33342 trihydrochloride, trihydrate (Thermo Fisher Scientific, USA). Sections were mounted using ProLong Gold Antifade (Thermo Fisher Scientific, USA). Sections not incubated with primary antibodies were used as controls. Images were taken using a confocal laser microscope (LSM 800, Zeiss, Germany).

Statistical Analysis

Data on ONL thickness measurements are presented as mean ± SEM, while ERG amplitudes and peak times are presented as mean ± SD. Statistical analysis was performed using ANOVA with Tukey *post hoc* tests using GraphPad software (v.8.2.1, GraphPad Software). The level of significance was set at 0.05.

SUPPLEMENTAL INFORMATION

Supplemental Information can be found online at https://doi.org/10.1016/j.stemcr.2020.12.007.

AUTHOR CONTRIBUTIONS

Conceptualization, X.S., T.A.B., B.V.S., and Z.L.; Methodology, G.L., B.V.S., X.S., V.A.B., G.S.W.T., and Z.L.; Investigation, X.S., T.A.B., B.H.P., Z.L., G.E.H., Q.S.W.T., D.S.L.W., K.H.O., W.Y., and W.H.; Writing – Original Draft, X.S., T.A.B., B.V.S., B.H.P., and Z.L.; Writing – Review & Editing, X.S., T.A.B., B.V.S., B.H.P., G.E.H., I.S., W.H., G.L., G.S.W.T., and Z.L.; Funding Acquisition, X.S.; Supervision, X.S. All authors reviewed and commented on the manuscript.

CONFLICTS OF INTEREST

Patent: EP2825108 (B.V.S.).

ACKNOWLEDGMENTS

This study was supported by IAF-PP (HMBS Domain) (OrBID: Ocular Biomaterials and Device), A*STAR, Singapore (H17/01/a0/013); a National University of Singapore start-up grant, Singapore (NUHSRO/2016/100/SU/01); and a National University Health System Clinical Scientist Program grant (Singapore) to X.S.; and by Hong Leong Endowed Professorship of the National University of Singapore funds (Singapore) to G.E.H. and B.V.S. We would like to acknowledge the veterinary team at the Translational Pre-clinical Model Platform (Singapore Eye Research Institute, Singapore) for providing support in NHP surgery preparation and animal follow-up.

Received: July 29, 2020
Revised: December 8, 2020
Accepted: December 10, 2020
Published: January 14, 2021

REFERENCES

Al-Nawaiseh, S., Thieltges, F., Liu, Z., Strack, C., Brinken, R., Braun, N., Wolschendorf, M., Maminishkis, A., Eter, N., and Stanzel, B.V. (2016). A step by step protocol for subretinal surgery in rabbits. J. Vis. Exp. https://doi.org/10.3791/53927.

Bharti, K., Miller, S.S., and Arnheiter, H. (2011). The new paradigm: retinal pigment epithelium cells generated from embryonic or induced pluripotent stem cells. Pigment Cell Melanoma Res. *24*, 21–34.

Bird, A.C., Phillips, R.L., and Hageman, G.S. (2014). Geographic atrophy: a histopathological assessment. JAMA Ophthalmol. *132*, 338–345.

Blenkinsop, T.A., Saini, J.S., Maminishkis, A., Bharti, K., Wan, Q., Banzon, T., Lotfi, M., Davis, J., Singh, D., Rizzolo, L.J., et al. (2015). Human adult retinal pigment epithelial stem cell-derived RPE monolayers exhibit key physiological characteristics of native tissue. Invest. Ophthalmol. Vis. Sci. *56*, 7085–7099.

Blenkinsop, T.A., Salero, E., Stern, J.H., and Temple, S. (2013). The culture and maintenance of functional retinal pigment epithelial monolayers from adult human eye. Methods Mol. Biol. *945*, 45–65.

Bonilha, V.L., Rayborn, M.E., Bhattacharya, S.K., Gu, X., Crabb, J.S., Crabb, J.W., and Hollyfield, J.G. (2006). The retinal pigment epithelium apical microvilli and retinal function. Adv. Exp. Med. Biol. *572*, 519–524.

Bovolenta, P., Mallamaci, A., Briata, P., Corte, G., and Boncinelli, E. (1997). Implication of OTX2 in pigment epithelium determination and neural retina differentiation. J. Neurosci. *17*, 4243–4252.

Charteris, D.G. (1995). Proliferative vitreoretinopathy: pathobiology, surgical management, and adjunctive treatment. Br. J. Ophthalmol. *79*, 953–960.

da Cruz, L., Fynes, K., Georgiadis, O., Kerby, J., Luo, Y.H., Ahmado, A., Vernon, A., Daniels, J.T., Nommiste, B., Hasan, S.M., et al. (2018). Phase 1 clinical study of an embryonic stem cell-derived retinal pigment epithelium patch in age-related macular degeneration. Nat. Biotechnol. *36*, 328–337.

Davis, R.J., Alam, N.M., Zhao, C., Muller, C., Saini, J.S., Blenkinsop, T.A., Mazzoni, F., Campbell, M., Borden, S.M., Charniga, C.J., et al. (2017). The developmental stage of adult human stem cell-derived retinal pigment epithelium cells influences transplant efficacy for vision rescue. Stem Cell Reports *9*, 42–49.

Diniz, B., Thomas, P., Thomas, B., Ribeiro, R., Hu, Y., Brant, R., Ahuja, A., Zhu, D., Liu, L., Koss, M., et al. (2013). Subretinal implantation of retinal pigment epithelial cells derived from human embryonic stem cells: improved survival when implanted as a monolayer. Invest. Ophthalmol. Vis. Sci. *54*, 5087–5096.

Fernandes, M., McArdle, B., Schiff, L., and Blenkinsop, T.A. (2018). Stem cell-derived retinal pigment epithelial layer model from adult human globes donated for corneal transplants. Curr. Protoc. Stem Cell Biol. *45*, e53.

Fields, M.A., Del Priore, L.V., Adelman, R.A., and Rizzolo, L.J. (2020). Interactions of the choroid, Bruch's membrane, retinal pigment epithelium, and neurosensory retina collaborate to form the outer blood-retinal-barrier. Prog. Retin. Eye Res. *76*, 100803.

Ilmarinen, T., Thieltges, F., Hongisto, H., Juuti-Uusitalo, K., Koistinen, A., Kaarniranta, K., Brinken, R., Braun, N., Holz, F.G., Skottman, H., et al. (2019). Survival and functionality of xeno-free human embryonic stem cell-derived retinal pigment epithelial cells on polyester substrate after transplantation in rabbits. Acta Ophthalmol. *97*, e688–e699.

Kashani, A.H., Lebkowski, J.S., Rahhal, F.M., Avery, R.L., Salehi-Had, H., Dang, W., Lin, C.M., Mitra, D., Zhu, D., Thomas, B.B., et al. (2018). A bioengineered retinal pigment epithelial monolayer for advanced, dry age-related macular degeneration. Sci. Transl Med. *10*, eaao4097.

Kashani, A.H., Uang, J., Mert, M., Rahhal, F., Chan, C., Avery, R.L., Dugel, P., Chen, S., Lebkowski, J., Clegg, D.O., et al. (2020). Surgical method for implantation of a biosynthetic retinal pigment epithelium monolayer for geographic atrophy: experience from a phase 1/2a study. Ophthalmol. Retina *4*, 264–273.

Liu, Z., Liow, S.S., Lai, S.L., Alli-Shaik, A., Holder, G.E., Parikh, B.H., Krishnakumar, S., Li, Z., Tan, M.J., Gunaratne, J., et al. (2019). Retinal-detachment repair and vitreous-like-body reformation via

a thermogelling polymer endotamponade. Nat. Biomed. Eng. *3*, 598–610.

Liu, Z., Yu, N., Holz, F.G., Yang, F., and Stanzel, B.V. (2014). Enhancement of retinal pigment epithelial culture characteristics and subretinal space tolerance of scaffolds with 200 nm fiber topography. Biomaterials *35*, 2837–2850.

Maeda, T., Lee, M.J., Palczewska, G., Marsili, S., Tesar, P.J., Palczewski, K., Takahashi, M., and Maeda, A. (2013). Retinal pigmented epithelial cells obtained from human induced pluripotent stem cells possess functional visual cycle enzymes in vitro and in vivo. J. Biol. Chem. *288*, 34484–34493.

Mandai, M., Watanabe, A., Kurimoto, Y., Hirami, Y., Morinaga, C., Daimon, T., Fujihara, M., Akimaru, H., Sakai, N., Shibata, Y., et al. (2017). Autologous induced stem-cell-derived retinal cells for macular degeneration. N. Engl. J. Med. *376*, 1038–1046.

Masuda, T., Wahlin, K., Wan, J., Hu, J., Maruotti, J., Yang, X., Iacovelli, J., Wolkow, N., Kist, R., Dunaief, J.L., et al. (2014). Transcription factor SOX9 plays a key role in the regulation of visual cycle gene expression in the retinal pigment epithelium. J. Biol. Chem. *289*, 12908–12921.

McCulloch, D.L., Marmor, M.F., Brigell, M.G., Hamilton, R., Holder, G.E., Tzekov, R., and Bach, M. (2015). ISCEV Standard for full-field clinical electroretinography (2015 update). Doc. Ophthalmol. *130*, 1–12.

Patteson, A.E., Vahabikashi, A., Pogoda, K., Adam, S.A., Mandal, K., Kittisopikul, M., Sivagurunathan, S., Goldman, A., Goldman, R.D., and Janmey, P.A. (2019). Vimentin protects cells against nuclear rupture and DNA damage during migration. J. Cell Biol. *218*, 4079–4092.

Salero, E., Blenkinsop, T.A., Corneo, B., Harris, A., Rabin, D., Stern, J.H., and Temple, S. (2012). Adult human RPE can be activated into a multipotent stem cell that produces mesenchymal derivatives. Cell Stem Cell *10*, 88–95.

Samuel, W., Jaworski, C., Postnikova, O.A., Kutty, R.K., Duncan, T., Tan, L.X., Poliakov, E., Lakkaraju, A., and Redmond, T.M. (2017). Appropriately differentiated ARPE-19 cells regain phenotype and gene expression profiles similar to those of native RPE cells. Mol. Vis. *23*, 60–89.

Schwartz, S.D., Hubschman, J.P., Heilwell, G., Franco-Cardenas, V., Pan, C.K., Ostrick, R.M., Mickunas, E., Gay, R., Klimanskaya, I., and Lanza, R. (2012). Embryonic stem cell trials for macular degeneration: a preliminary report. Lancet *379*, 713–720.

Schwartz, S.D., Regillo, C.D., Lam, B.L., Eliott, D., Rosenfeld, P.J., Gregori, N.Z., Hubschman, J.P., Davis, J.L., Heilwell, G., Spirn, M., et al. (2015). Human embryonic stem cell-derived retinal pigment epithelium in patients with age-related macular degeneration and Stargardt's macular dystrophy: follow-up of two open-label phase 1/2 studies. Lancet *385*, 509–516.

Sharma, R., Khristov, V., Rising, A., Jha, B.S., Dejene, R., Hotaling, N., Li, Y., Stoddard, J., Stankewicz, C., Wan, Q., et al. (2019). Clinical-grade stem cell-derived retinal pigment epithelium patch rescues retinal degeneration in rodents and pigs. Sci. Transl Med. *11*, eaat5580.

Singh, M.S., Park, S.S., Albini, T.A., Canto-Soler, M.V., Klassen, H., MacLaren, R.E., Takahashi, M., Nagiel, A., Schwartz, S.D., and Bharti, K. (2020). Retinal stem cell transplantation: Balancing safety and potential. Prog. Retin. Eye Res. *75*, 100779.

Sparrow, J.R., Hicks, D., and Hamel, C.P. (2010). The retinal pigment epithelium in health and disease. Curr. Mol. Med. *10*, 802–823.

Stanga, P.E., Kychenthal, A., Fitzke, F.W., Halfyard, A.S., Chan, R., Bird, A.C., and Aylward, G.W. (2002). Retinal pigment epithelium translocation after choroidal neovascular membrane removal in age-related macular degeneration. Ophthalmology *109*, 1492–1498.

Stanzel, B., Ader, M., Liu, Z., Amaral, J., Aguirre, L.I.R., Rickmann, A., Barathi, V.A., Tan, G.S.W., Degreif, A., Al-Nawaiseh, S., et al. (2019). Surgical approaches for cell therapeutics delivery to the retinal pigment epithelium and retina. Adv. Exp. Med. Biol. *1186*, 141–170.

Stanzel, B.V., Liu, Z., Brinken, R., Braun, N., Holz, F.G., and Eter, N. (2012). Subretinal delivery of ultrathin rigid-elastic cell carriers using a metallic shooter instrument and biodegradable hydrogel encapsulation. Invest Ophthalmol. Vis. Sci. *53*, 490–500.

Stanzel, B.V., Liu, Z., Somboonthanakij, S., Wongsawad, W., Brinken, R., Eter, N., Corneo, B., Holz, F.G., Temple, S., Stern, J.H., et al. (2014). Human RPE stem cells grown into polarized RPE monolayers on a polyester matrix are maintained after grafting into rabbit subretinal space. Stem Cell Reports *2*, 64–77.

Strauss, O. (2005). The retinal pigment epithelium in visual function. Physiol. Rev. *85*, 845–881.

Sugita, S., Mandai, M., Hirami, Y., Takagi, S., Maeda, T., Fujihara, M., Matsuzaki, M., Yamamoto, M., Iseki, K., Hayashi, N., et al. (2020). HLA-matched allogeneic iPS cells-derived RPE transplantation for macular degeneration. J. Clin. Med. *9*, 2217.

Thieltges, F., Liu, Z., Brinken, R., Braun, N., Wongsawad, W., Somboonthanakij, S., Herwig, M., Holz, F.G., and Stanzel, B.V. (2016). Localized RPE removal with a novel instrument aided by viscoelastics in rabbits. Transl Vis. Sci. Technol. *5*, 11.

van Zeeburg, E.J., Maaijwee, K.J., Missotten, T.O., Heimann, H., and van Meurs, J.C. (2012). A free retinal pigment epithelium-choroid graft in patients with exudative age-related macular degeneration: results up to 7 years. Am. J. Ophthalmol. *153*, 120–127.e2.

Wong, W.L., Su, X., Li, X., Cheung, C.M., Klein, R., Cheng, C.Y., and Wong, T.Y. (2014). Global prevalence of age-related macular degeneration and disease burden projection for 2020 and 2040: a systematic review and meta-analysis. Lancet Glob. Health *2*, e106–116.

Yeaman, C., Grindstaff, K.K., and Nelson, W.J. (1999). New perspectives on mechanisms involved in generating epithelial cell polarity. Physiol. Rev. *79*, 73–98.